Contents lists available at ScienceDirect

Journal of Membrane Science

Immobilization of silver nanoparticle-decorated silica particles on polyamide thin film composite membranes for antibacterial properties

Sang-Hee Park [a,b], Young-Seon Ko [c], Sung-Joon Park [a], Jong Suk Lee [d], Jinhan Cho [a], Kyung-Youl Baek [b,e], Il Tae Kim [f], Kyoungja Woo [c,*], Jung-Hyun Lee [a,**]

[a] Department of Chemical and Biological Engineering, Korea University, 5-1 Anam-dong, Seongbuk-gu, Seoul 136-713, Republic of Korea
[b] Materials Architecturing Research Center, Korea Institute of Science and Technology, 39-1 Hawolgok-dong, Seongbuk-gu, Seoul 136-791, Republic of Korea
[c] Nanophotonics Research Center, Korea Institute of Science and Technology, 39-1 Hawolgok-dong, Seongbuk-gu, Seoul 136-791, Republic of Korea
[d] Center for Environment, Health and Welfare Research, Korea Institute of Science and Technology, 39-1 Hawolgok-dong, Seongbuk-gu, Seoul 136-791, Republic of Korea
[e] KIST-UNIST-Ulsan Center for Convergence Materials, 50 UNIST-gil, Eonyang-eup, Ulju-gun, Ulsan 689-698, Republic of Korea
[f] Department of Chemical and Biological Engineering, Gachon University, 1342 Seongnamdaero, Sujeong-gu, Gyeonggi-do 461-701, Republic of Korea

ABSTRACT

We present a new strategy to strongly and effectively immobilize silver nanoparticles (AgNPs) on polyamide thin film composite membranes to endow antibacterial activity. This method relies on the immobilization of relatively large silica particles (SiO_2, $\sim$400 nm in diameter), where AgNPs of $\sim$30 nm in diameter are tightly and densely bound ($AgNP@SiO_2$), on the membrane surface using cysteamine as a covalent linker. The formation of multiple Ag–S chemical bonds between a "bumpy" $AgNP@SiO_2$ and the rough membrane surface provides a great leaching stability of AgNPs and $AgNP@SiO_2$. $AgNP@SiO_2$ particles were well distributed over the entire membrane surface without severe aggregation. The surface coverage of the membrane by $AgNP@SiO_2$ was tuned by adjusting the deposition time and $AgNP@SiO_2$ particle concentration. The $AgNP@SiO_2$-immobilized membrane showed excellent antibacterial properties against *Escherichia coli*, *Pseudomonas aeruginosa* and *Staphylococcus aureus,* even with a relatively low particle coverage. Importantly, the separation performance (water flux and salt rejection) of the membrane was not impaired by particle immobilization. These beneficial effects are attributed mainly to the sparse and good distribution of $AgNP@SiO_2$, which can reinforce the antibacterial activity of AgNPs while having a negligible impact on the hydraulic resistance.

1. Introduction

With the increasing global demand for clean water, membrane separation process such as reverse osmosis (RO) and nanofiltration (NF) has become a leading technology for seawater desalination and water treatment [1]. A polyamide (PA) thin film composite (TFC) membrane consisting of a PA selective layer ($\sim$100 nm in thickness) on top of an asymmetrically porous polymer support is currently the predominant membrane material for RO and NF applications due to its high salt rejecting ability and excellent chemical/physical stability [2]. Despite such merits, the PA TFC membrane suffers from severe biofouling, which hampers further reduction of the operation and maintenance costs of the

membrane process [3].

Biofouling arises from the undesired formation of biofilm on the membrane surface *via* the deposition, growth and metabolism of microorganisms, particularly bacteria, which seriously reduces the water flux and thus the lifetime of the membrane [4,5]. Chlorine and its derivatives have been commonly used as disinfectants to control membrane biofouling [6]. However, chlorine-based disinfectants are known to degrade the membrane performance by destroying the amide bonding of the PA selective layer [7]. In addition, it is impossible to completely remove the bacteria by various pretreatments and to maintain the bacteria-free condition due to the self-replicating nature of the survived bacteria [8].

Incorporating biocidal nanomaterials into the membranes has proven effective for reducing the membrane biofouling [9]. A variety of biocidal nanomaterials such as silver nanoparticles (AgNPs) or silver ions (Ag^+) [10,11], copper nanoparticles (CuNPs) or cupric ions (Cu^{2+}) [12], titanium dioxides (TiO_2) [13], zinc

oxides (ZnO) [14] and carbonaceous materials [15], have been incorporated into the membranes through *in-situ* blending, coating and immobilization. Among these materials, AgNPs and Ag$^+$ ions have been extensively studied as biocidal agents to effectively mitigate the membrane biofouling because of their strong and broad-spectrum antimicrobial activities for bacteria, fungi and viruses [16]. Although various strategies have been developed to incorporate AgNPs into the membranes [17], recent studies have mainly focused on devising methods to immobilize AgNPs on the membrane surface to ensure direct, effective and long-lasting antibacterial activity. For example, polyelectrolyte-capped AgNPs were successfully immobilized on commercial TFC membranes *via* polyelectrolyte layer-by-layer assembly [18]. Zhang et al. also strongly bound AgNPs on the PEGylated dendrimer-grafted TFC membrane surface [19]. Furthermore, it was reported by Yin et al. that AgNPs could be immobilized on the PA TFC membrane surface functionalized with cysteamine ($NH_2-(CH_2)_2-SH$) through the formation of strong Ag–S bonding [20].

While most immobilization strategies reported to date have effectively imparted excellent antibacterial properties to the membranes, the formation of undesirable NP aggregates resulting from their strong coagulating nature has been recognized as one of the most critical issues. For example, although the use of the pristine AgNPs without capping agents or stabilizers is desirable to intensify antibacterial activity as well as enhance immobilization efficiency, the tendency to form NP aggregates is further accelerated. Severe NP aggregation can increase the hydraulic resistance of the membrane due to the excess of deposited NPs [21,22]. This also can lead to the unwanted elution of loosely-bound NP aggregates during the membrane operation, which may have a detrimental effect on human health and the environment. In addition, the previously reported immobilization methods often resulted in the deterioration of membrane performance, such as a reduction in salt rejection or water flux [18,20,22]. These challenging issues have motivated us to design and exploit an approach to effectively immobilize NPs for high performance and durable TFC membranes.

Here, we introduce a new strategy to strongly and effectively immobilize uncapped, pristine AgNPs on the PA TFC membrane surface without compromising membrane performance. This approach is based on the attachment of AgNP–SiO$_2$ hybrid particles (AgNP@SiO$_2$), in which AgNPs ($\sim$30 nm in diameter) were robustly and uniformly grown on the aminopropyl moiety-functionalized SiO$_2$ particles ($\sim$400 nm in diameter), to the membrane surface. The PA TFC membrane surface was functionalized with thiol groups by pretreating with cysteamine in a manner that does not deteriorate the membrane performance. Then, AgNP@SiO$_2$ particles were tightly immobilized *via* forming multiple Ag–S bonds between the particle and the membrane, which could promote the stability of AgNP@SiO$_2$ against leaching. The use of relatively large AgNP@SiO$_2$ particles provides several key advantages over direct deposition of AgNPs: *i.e.,* Minimal aggregation of AgNP@SiO$_2$ consequently allows the good and effective distribution of AgNPs over the entire membrane surface, imparting an excellent antibacterial activity to the membrane with minimum loading of AgNP@SiO$_2$, which in turn has negligible effect on the membrane permeation.

2. Experimental

2.1. Materials

Ammonium hydroxide (NH$_4$OH, 28.0–30.0%, Junsei), tetrakis (hydroxymethyl) phosphonium chloride (80% solution in water, Sigma-Aldrich), formaldehyde (37% solution in 10–15% methanol, Sigma-Aldrich), silver nitrate (AgNO$_3$, 99.0%, Sigma-Aldrich), sodium hydroxide (NaOH, 93.0%, Showa) and hydrochloric acid (HCl, 35%, Matsunoen Chemicals Ltd.) were used as-purchased. Polysulfone (PSf) ultrafiltration (UF) membrane (PS-20) as a support was purchased from ULTURA, Inc. Trimesoyl chloride (TMC, 98%, Sigma-Aldrich), *m*-phenylenediamine (MPD, 99%, Sigma-Aldrich), cysteamine (98%, Sigma-Aldrich), isopropyl alcohol (99.7%, J.T. Baker), *n*-hexane (95%, J.T. Baker), potassium hydroxide (KOH, 85%, Daejung Chemical), potassium carbonate (K$_2$CO$_3$, 99.5%, Daejung Chemical), 4-dimethylaminopyridine (DMAP, 99%, Daejung Chemical), nitric acid (HNO$_3$, 60%, Daejung Chemical), sodium chloride (NaCl, 99%, Daejung Chemical), phosphate buffered saline (PBS, Sigma-Aldrich), Luria-Bertani (LB) broth miller (BD DifcoTM) and agar (extra pure, Daejung Chemical) were used without further purification. De-ionized (DI) water (18.2 MΩ cm) was prepared in a Millipore purification system. *Escherichia coli* (*E. coli*, ATCC 47076) was obtained from American Type Culture Collection. *Pseudomonas aeruginosa* (*P. aeruginosa*, KCTC 2004) and *Staphylococcus aureus* (*S. aureus*, KCTC 3881) were received from Korean Collection for Type Cultures.

2.2. Synthesis of AgNP@SiO$_2$ particles

The AgNP@SiO$_2$ particles were prepared according to the previously reported method [23] with some optimization for a smaller scale. First, 10 mL of aqueous solution containing 2.45 g of aminopropyl-functionalized silica (AP-SiO$_2$, $\sim$400 nm in diameter, 3.66×10^{13} particles) prepared by our published protocol [23] was mixed with 31 mL of 0.1 M HCl to adjust the solution pH to $\sim$4, and stirred for 15 h to ensure a homogeneous dispersion. For the preparation of Ag seeds, 0.384 mL of tetrakis(hydroxymethyl) phosphonium chloride was dissolved in 0.8 L of 0.01 M NaOH solution. To this solution, 32 mL of 1 wt% of AgNO$_3$ aqueous solution was added, and the mixture was stirred at room temperature for 15 min. The pH-adjusted AP-SiO$_2$ solution was mixed with the Ag seed solution to self-assemble Ag seeds on the AP-SiO$_2$ and gently swirled every 30 min for 2 h. The unbound Ag seeds were removed using centrifugation and the Ag-seeded SiO$_2$ solid was dispersed in 30 mL of DI water. The solution was poured into the mixture of AgNO$_3$ (2.6 g) and NH$_4$OH (30 wt% in water, 5.2 mL) in 4.5 L of DI water at 12 $\pm$ 1 °C in an ice bath and stirred for 20 min with a mechanical stirrer to sort out the relatively larger seeds. Then, 3.5 mL of formaldehyde dissolved in 300 mL DI water was slowly injected into the reaction mixture as a reducing reagent. After further stirring for 2 h, the resulting AgNP@SiO$_2$ particles were purified with DI water using centrifugation and dispersed in 300 mL of DI water. The solution (10 mL) was fully dried to give 0.15 g of AgNP@SiO$_2$, with a total estimated yield of 4.5 g. The particle number concentration of AgNP@SiO$_2$ was traced assuming a yield of unity based on silica particles because most of the particles could be collected by centrifugation. For the growing solution, the molar ratio of NH$_4$OH/AgNO$_3$ was twice as high as the published method [23]. This increased ratio consistently provided a well-dispersed AgNP@SiO$_2$ solution.

2.3. Fabrication of membranes

A PA selective layer was hand-cast onto a commercial PSf UF membrane support *via* interfacial polymerization. Before the reaction, organic contaminants on the PSf membrane surface were cleaned with isopropyl alcohol for 10 min and immersed in DI water for 15 min. A 3.0 wt% MPD aqueous solution was poured on the cleaned PSf membrane support which had been fixed with silicone frames. After impregnation for 3 min, the excess MPD solution was removed by an air knife. Next, a 0.1 wt% TMC/*n*-hexane solution was spread over the membrane impregnated with

MPD and allowed to react at room temperature for 1 min to produce a PA selective layer. The TMC solution was drained off, and then the membrane was rinsed with pure n-hexane to complete the reaction and remove the unreacted TMC.

The prepared PA TFC membrane was further functionalized with cysteamine to prepare the thiol-functionalized TFC membrane (TFC-SH). The functionalization process utilizes amide formation reaction between acyl chloride groups on the PA TFC membrane surface and amine groups of cysteamine in an aqueous phase at room temperature. The optimized base solution (pH=12) was used to circumvent the hydrolysis of acyl chloride during the amide formation reaction [24]. DMAP (0.122 g, 1 mmol) and K_2CO_3 (2.08 g, 15 mmol) were first dissolved in 20 mL of DI water. A 5 M KOH aqueous solution was slowly added to the solution to adjust the pH to 12. The aqueous mixture was stirred after adding cysteamine of different concentrations (2, 5, 10, 15 and 20 mmol). The prepared cysteamine aqueous solution was contacted with the surface of the PA TFC membrane immediately after the last rinsing step of the membrane fabrication to prevent the hydrolysis of acyl chloride in air. The reaction was allowed to proceed for 30 min and was terminated by rinsing with DI water several times.

Immobilization of AgNP@SiO_2 particles on the TFC-SH membrane was performed as follows. One hundred mL of the AgNP@SiO_2 aqueous suspension was sonicated at 25 °C for 3 s and then agitated using a rotational shaker at 20 rpm for 24 h to ensure a uniform dispersion of AgNP@SiO_2 particles in water. The TFC-SH membrane (5×5 cm^2) was placed on the interior side of the lid of a glass jar holding 100 mL of the AgNP@SiO_2 aqueous suspension. The membrane was contacted with the AgNP@SiO_2 suspension by turning the jar upside down for various periods of time (3, 6, 12, 24 and 36 h). The concentration of AgNP@SiO_2 suspension was controlled at 1.5, 4.5, 7.5, 15.0 and 22.5×10^8 particles mL^{-1}. After deposition, excess and loosely-bound AgNP@SiO_2 particles were removed by thoroughly rinsing with DI water to obtain the AgNP@SiO_2-immobilized TFC membrane (TFC-AgNP@SiO_2). All the prepared membranes (pristine TFC, TFC-SH and TFC-AgNP@SiO_2) were stored in DI water prior to use.

2.4. Characterization of AgNP@SiO_2 particles and membranes

The size and morphology of the synthesized AgNP@SiO_2 particles were analyzed by transmission electron microscopy (TEM, CM30, Philips) and SEM (Inspect F50, FEI). The surface and cross-sectional morphology of the membranes were examined using SEM. All the SEM samples were coated with Pd/Pt for 20 s (E-1010 Ion Sputter, HITACHI) and imaged at an accelerating voltage of 10 kV. The particle surface coverage of the TFC-AgNP@SiO_2 membrane was estimated from SEM images using ImageJ software. XPS and FT-IR were used to characterize the chemical structures of the membranes. XPS was performed on a PHI-5000 Versaprobe spectrometer using monochromatized Al K$_\alpha$ radiation at 1486.6 eV. FT-IR spectra were collected on a Nicolet IS10 spectrometer (Thermo Scientific) equipped with an attenuated total reflectance (ATR) unit. A goniometer (NRL CA Goniometer, Rame-Hart Inc.) equipped with a video capture camera was employed to measure the water contact angles of the membranes. The average values of contact angles were obtained from at least 7 measurements for each sample.

2.5. Evaluation of membrane performance

The separation performance (water flux and NaCl rejection) of the prepared membranes was evaluated using a cross-flow filtration apparatus with an effective membrane area of 12.4 cm^2 (A). Performance test was carried out using NaCl aqueous solution (2000 mg L^{-1}) at an operating pressure of 15.5 bar and a flow rate

of 1 L min^{-1}. Performance data were collected after a compaction time of 3 h, which allowed the system to reach a steady state. The water flux (J_w, L m^{-2} h^{-1}) was calculated by measuring the volume of water permeate (ΔV) through the fixed membrane area for a certain time interval (Δt), as given by,

$$J_w = \frac{\Delta V}{A \, \Delta t} \tag{1}$$

The NaCl rejection (R, %) was determined by measuring the NaCl concentrations of the feed (C_f) and permeate (C_p) solutions which were measured with a conductivity meter (Cond 730P, IN-OLAB), as the following equation,

$$R = 100 \times \frac{(C_f - C_p)}{C_f} \tag{2}$$

2.6. Assessment of membrane antibacterial activity

The antibacterial properties of the membranes were assessed for three model bacteria, *E. coli*, *P. aeruginosa* and *S. aureus*, by the viable cell attachment test following the previously reported protocol [10,20]. The bacteria were grown in LB with shaking at 37 °C overnight. Then, the prepared bacteria solution was diluted in fresh LB broth and incubated further for 3 h. The bacteria culture was centrifuged at 13,500 rpm for 1 min and then, the separated bacteria were re-dispersed in a 10 mM PBS solution (pH=7.4) containing 0.138 M NaCl and 0.00027 M KCl. The bacteria solutions were diluted to the following specific concentrations: 10^8 colony forming units (CFU) mL^{-1} for *E. coli* and 10^6 CFU mL^{-1} for *P. aeruginosa* and *S. aureus*. Each membrane sample of 4 cm^2 was placed into each bacteria solution and cultured while shaking at 250 rpm and at 37 °C for 2 h. The incubated membranes were cleaned with a PBS solution twice to remove the unattached bacteria from the membrane surface. Then, the bacteria attached on the membrane surface were separated by sonicating (using a bath sonicator, 70 W, 20 kHz) the membrane in 10 mL of a sterile PBS buffer solution for 7 min. It was confirmed that this sonication condition is strong enough to detach all the bacteria adhering to the membrane surface without damaging the bacteria (see the Supporting information S1 and S2). The obtained bacteria solution was diluted with a PBS solution and spread on LB agar plates. The number of CFUs on each plate was counted after incubation at 37 °C for 12 h. This protocol allows the assessment of the antibacterial activity on the membrane surface, which directly accounts for the ability of restricting biofilm growth and thus mitigating biofouling occurring on the membrane surface.

Additionally, the membrane antibacterial effect in the bacteria solutions was evaluated by following the previously reported protocol [25,26]. After removing the membranes from the above incubated bacteria solutions, the remaining supernatant solutions were diluted and then, spread on nutrient agar plates, followed by culturing at 37 °C for 24 h. The blank control solution (without being contacted with the membrane) was also incubated with the sample protocol. The number of CFUs on each plate was counted to calculate the percent bacterial viability in the solutions as follows [25,26],

$$\text{Bacterial viability } (\%) = 100 \frac{N}{N_0} \tag{3}$$

where N is the colony count of the bacteria cultures contacted with membranes and N_0 is the colony count of the blank control culture.

Live and dead bacteria on the membrane surface were also identified by fluorescence microcopy images. The membranes incubated in bacteria solutions were thoroughly washed with phosphate buffer to remove the unbound bacteria on the

membrane surface, and then stained with SYTO 9 and propidium iodide (PI) of the Live/Dead *Bac*Light bacterial viability kit (Molecular Probes, Willow Creek, OR, USA) at room temperature for 30 min. After staining, the membrane samples were carefully washed twice with phosphate buffer to remove residual dyes. The bacteria were examined using confocal laser scanning microscopy (CLSM) (Carl Zeiss LSM700, Jena, Germany). The fluorescent filters had the following excitation and emission wavelengths (SYTO 9: 480 and 500 nm; PI: 490 and 635 nm). CLSM images were obtained using a $40 \times$ objective lens (C-APOCHROMAT/1.20 W Korr M27, Carl Zeiss) and analyzed by the Zen 2012 program (Carl Zeiss).

2.7. Releasing test of silver ions (Ag^+) of the TFC-AgNP@SiO$_2$ membrane

The releasing rate of Ag^+ ions from the TFC-AgNP@SiO$_2$ membrane was evaluated with a batch experiment by adopting the protocol reported by Yin et al. [20]. The TFC-AgNP@SiO$_2$ membrane coupon of 4 cm^2 was immersed in a bottle containing 20 mL of DI water, which was agitated on the rotator (AG, FI-NEPCR) at 50 rpm. The solution was replaced with fresh DI water every 24 h. The collected solution was acidified using a 1 wt% HNO$_3$ aqueous solution and then analyzed by inductively coupled plasma mass spectrometry (ICP-MS, NEXION 300D, PerkinElmer) to determine its Ag content. Another 4 cm^2 piece of the TFC-AgNP@SiO$_2$ membrane was immersed into a 1 wt% HNO$_3$ aqueous solution and sonicated for 10 min, which allows all the AgNPs attached on the membrane to be dissolved completely. The collected supernatant solution was analyzed by ICP-MS to quantify the total amount of Ag loaded on the membrane.

3. Results and discussion

3.1. AgNP@SiO$_2$ particles

Fig. 1 shows the SEM and TEM images of the synthesized AgNP@SiO$_2$ particles, which exhibit a uniform size ($\sim$400 nm in diameter) and morphology. Spherical AgNPs are densely and uniformly bound on the AP-SiO$_2$ particle surface without forming any AgNP aggregates. The size of the AgNPs was estimated to range from 10 to 50 nm in diameter with the major sizes over $\sim$30 nm. The relatively large size and thus small surface to volume ratio of the AgNP@SiO$_2$ particles are favorable to minimize particle aggregation during the immobilization process [27]. A low propensity for forming aggregates would in turn prevent a significant increase in the hydraulic resistance of the membrane caused by excess particle deposition [21].
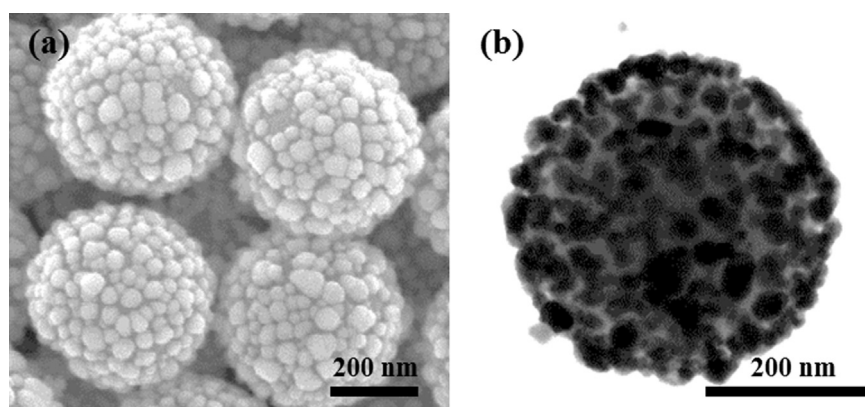
3.2. AgNP@SiO$_2$-immobilized PA TFC membranes

The schematic of the immobilization of AgNP@SiO$_2$ particles on the membrane is illustrated in Fig. 2. First, a pristine TFC membrane is treated with cysteamine to functionalize its surface with thiol groups (–SH), which subsequently are chemically linked with AgNPs existing on the AgNP@SiO$_2$ particles. Cysteamines are covalently bound to the membrane surface *via* the amide formation reaction of their amine groups with acyl chlorides on the membrane surface. During the amide formation, thioesters can be formed between the thiol groups of cysteamine and the acyl chlorides on the membrane surface. However, the amides are preferentially produced due to the well-known transfer of the acyl group to the amine group of cycteamine [29].The recently reported protocol to functionalize a PA TFC membrane with cysteamine relies on the amide formation reaction in alcohol media, which can facilitate the amide formation by retarding the hydrolysis of acyl chloride to the less reactive carboxylic acid [20]. However, alcohols can have an adverse influence on the membrane performance (particularly loss of selectivity) by severely swelling and loosening the PA chain network [28]. To prevent the hydrolysis of acyl chloride and the solvent-induced PA damage simultaneously, the cysteamine treatment was performed in aqueous media under the optimized base condition as described above.

The successful membrane functionalization with cysteamine was verified by XPS and FT-IR chemical analysis. Fig. 3a shows the XPS spectra corresponding to sulfur (S2p) of the TFC-SH as a function of cysteamine concentrations at a fixed deposition time (30 min). The presence of the S2p peak at 164 eV results from the thiol groups of cysteamine which was deposited on the pristine TFC membrane surface [30]. The deposition time was predetermined to be 30 min when the intensity of the S2p XPS peak reached a plateau. The S2p peak became more pronounced as the cysteamine concentration increased. The sulfur contents determined from the S2p peak intensities of the TFC-SH membranes are plotted as a function of cysteamine concentrations in Fig. 3b. The sulfur content progressively increased with increasing the cysteamine concentration up to 10 mmol and then leveled off to $\sim$0.5%, indicating that 10 mmol of cysteamine is a sufficient concentration to functionalize the membrane surface with a maximum amount of thiol groups. Hence, we fixed the cysteamine concentration to 10 mmol for all of the membrane modification processes. The FT-IR spectra of the pristine TFC and TFC-SH membranes show four characteristic absorbance peaks in the range of 3000–2800 cm^{-1} (Fig. 3c), which are associated with aliphatic –CH stretching. The peaks at 2967 and 2872 cm^{-1} are assigned to asymmetric and symmetric –CH stretching of the methyl group (–CH$_3$), respectively, while the peaks at 2928 and 2856 cm^{-1} are associated with asymmetric and symmetric –CH

Fig. 1. (a) SEM and (b) TEM images of AgNP@SiO$_2$ particles.

Fig. 2. Schematic illustration of the immobilization of AgNP@SiO$_2$ particles on a PA TFC membrane.

stretching of the methylene group (–CH$_2$–), respectively [31]. The intensity of the methylene peak (at 2928 cm^{-1}) relative to that of the methyl peak (at 2967 cm^{-1}) is more pronounced for the TFC-SH membrane, indicating the deposition of cysteamine having two methylene groups on the membrane.

Importantly, the amide bond formation between the amine of cysteamine and acyl chloride of the PA membrane is evidenced by the high-resolution XPS spectra of the pristine TFC and TFC-SH membranes. The XPS spectra of C1s and O1s were deconvoluted to identify the chemical environments around carbon and oxygen atoms. The deconvoluted C1s and O1s peaks are presented in Fig. 4 and their area percentages are summarized in Table 1.

The deconvoluted C1s peaks appear at binding energies of 285.0 eV (C1: aliphatic/aromatic C–C or C–H), 286.0 eV (C2: C–O or C–N), 288.4 eV (C3: C=O or O=C–N of amide), and 289.0 eV (C4: O=C–O of carboxyl group) for both pristine TFC and TFC-SH membranes [32,33]. The O1s spectrum was deconvoluted to two peaks at 532.1 eV (O1: C=O, C–O or O=C–N of amide) and 533.3 eV (hydrogen bonded O=C–N or O=C–O of carboxyl group) for both membranes [32,33]. It was found that the area percentage ratios of C3/C4 and O1/O2 (indicating the ratio of O=C–N of amide/O=C–O of carboxylic group) are larger for the TFC-SH compared to that of the pristine TFC. The relative increase in the amount of amide groups for the TFC-SH implies that cysteamine was covalently bound on the membrane surface through forming the amide bond between the amine and acyl chloride.

Fig. 5 shows the surface and cross-sectional morphologies of the pristine TFC and TFC-AgNP@SiO$_2$ membranes. The pristine TFC exhibits the "ridge and valley" structure, which is typical of the interfacially polymerized PA (inset of Fig. 5a). For the TFC-AgNP@SiO$_2$ membrane, AgNP@SiO$_2$ particles are fairly well distributed over the entire membrane surface although aggregates of a few particles are still visible (Fig. 5b). As a result, this morphology allows the good distribution of AgNPs, which is not readily achievable with conventional direct deposition of uncapped AgNPs. It should be noted that direct immobilization of

uncapped AgNP on the membrane surface typically leads to the formation of severe NP aggregates (see the Supporting information S3). The stability of the AgNP@SiO$_2$ particles were evaluated by examining the membrane surfaces before and after the RO performance test (at 15.5 bar for 48 h). The detachment of AgNPs from the AgNP@SiO$_2$ particles was not noticeable after the performance test (insets of Fig. 5b and c), which could be attributed to the robust fixation of AgNPs by embedding aminopropyl moieties covalently bound to the silica surface [23,34]. In addition, the AgNP@SiO$_2$ aggregates remained intact without breaking apart (insets of Fig. 5b and c), indicating strong inter-particle adhesion, likely resulting from the increased contact area between "bumpy" particles. Importantly, most AgNP@SiO$_2$ particles remained adhered to the membrane surface, with their surface coverage nearly unchanged after the performance test. Even extending filtration time up to 150 h did not alter the surface coverage (see the Supporting information S4). This observation demonstrates the excellent stability of AgNP@SiO$_2$ against detachment, which is imparted presumably by the strong Ag–S bond between the AgNPs bound to AgNP@SiO$_2$ and the thiol groups on the TFC-SH membrane surface [35]. The cross-sectional image revealed that AgNP@SiO$_2$ particles are wrapped with the ridge and valley structure of the PA layer (Fig. 5d). Such a unique geometrical feature could increase the contact area of the AgNP@SiO$_2$ particle and thus form multiple Ag–S bonds between the particle and the membrane surface, enhancing the adhesion force of AgNP@SiO$_2$ with the membrane surface. This multiple contact mechanism for the high stability of the relatively large AgNP@SiO$_2$ particle is analogous to the case of natural pollen grains whose spiky structures reinforce van der Waals adhesion with various surfaces by allowing multiple contacts [36]. To further verify our hypothesis, SiO$_2$ support particles were selectively removed from the membrane surface by applying controlled sonication. The region covered by concentrated AgNPs (denoted as a dotted circle in Fig. 5e) is regarded as the traces of AgNPs previously attached to the membrane before sonication, which supports our proposed
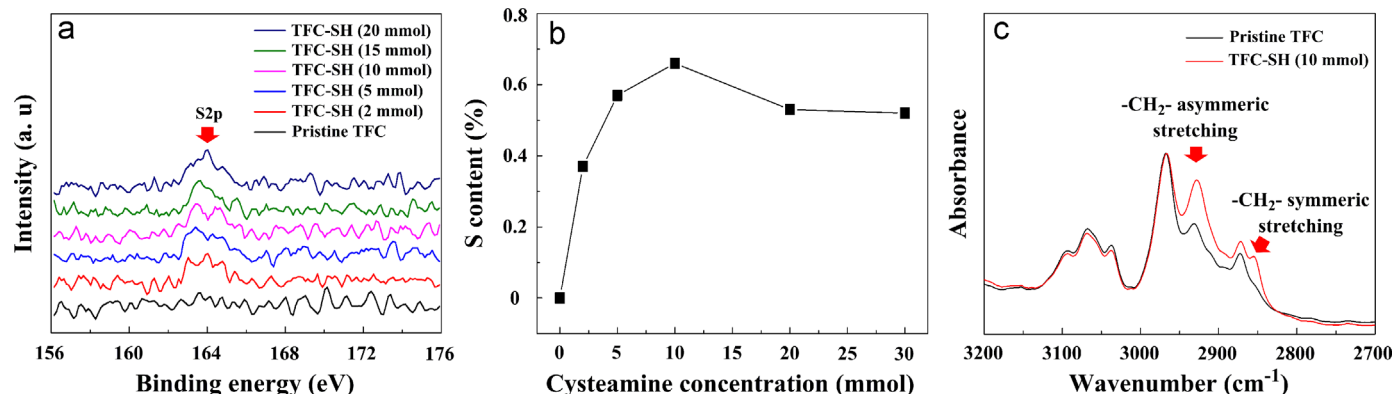
Fig. 3. (a) XPS sulfur (S2p) spectra and (b) corresponding sulfur contents of the TFC-SH membranes as a function of cysteamine concentrations used in functionalization. (c) FT-IR spectra of the pristine TFC and TFC-SH membranes. All the TFC-SH samples were prepared with constant deposition time of 30 min.
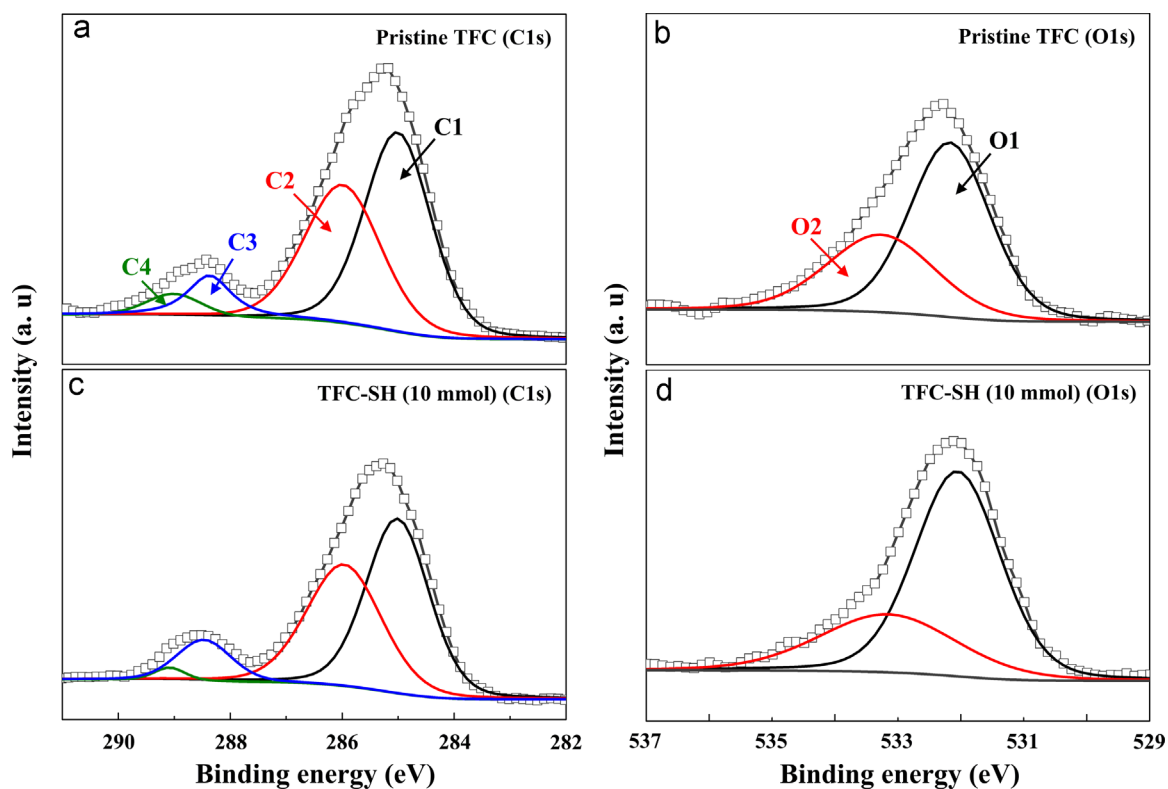
Fig. 4. High resolution XPS spectra of (a) C1s and (b) O1s peaks of the pristine TFC membrane and (c) C1s and (d) O1s peaks of the TFC-SH membrane.

Table 1
Binding energies and area percentages of deconvoluted XPS C1s and O1s peaks of the pristine TFC and TFC-SH membranes.

Band[a]	Binding energy (eV)	Peak assignment	Area percentage of peaks (%)	
			Pristine TFC	TFC-SH (10 mmol)
C1	285.0	C–C, C–H	48.3	50.2
C2	286.0	C–O, C–N	38.7	58.3
C3	288.4	C=O, O=C–N	8.7	10.0
C4	289.0	O=C–O	4.3	1.5
O1	532.1	O=C–N, C=O, C–O	62.8	68.9
O2	533.3	H–O=C–N, O=C–O	37.2	31.1

[a] From ref. [32,33].

mechanism that AgNP@SiO$_2$ is strongly bound on the membrane *via* forming multiple Ag–S bonds. In addition, the embedded morphology of the AgNP@SiO$_2$ within the ridge-and-valley PA structure could further enhance the stability by reducing the particle area exposed to shear flow during performance test.

The surface coverage of the membrane by AgNP@SiO$_2$ can be effectively controlled by adjusting the particle deposition time and particle concentration. Fig. 6 represents the particle surface coverage of the membrane as a function of the particle deposition time and particle concentrations. At a fixed particle concentration of 7.5×10^8 particles mL^{-1}, the surface coverage increased progressively with increasing the deposition time up to 24 h and then reached a steady value of $11 \pm 1\%$ (Fig. 6a). The relatively slow deposition rate is likely to be associated with the unique adhesion mechanism of AgNP@SiO$_2$. As discussed above, the strong immobilization of large AgNP@SiO$_2$ particles is presumably achieved *via* multiple chemical bonding when the geometrical condition (particle wrapping with rough PA features) is met. Although the

thiol group has a strong affinity with AgNP [37], a sufficient deposition time ($\sim$24 h) would be required for AgNP@SiO$_2$ particle to find the proper site allowing multiple contacts that ensure the strong particle-membrane adhesion. Fig. 6b shows the effect of particle concentration on the particle surface coverage of the membrane. The surface coverage increased gradually with increasing the particle concentration up to 7.5×10^8 particles mL^{-1}, and then increased sharply to the value of $\sim$35% until the particle concentration increased to 22.5×10^8 particles mL^{-1}. The enhanced increasing rate of the surface coverage for high particle concentrations ($> 7.5 \times 10^8$ particles mL^{-1}) is attributed to the extensive formation of AgNP@SiO$_2$ aggregates (inset of Fig. 6b) resulting from the intensified inter-particle attraction [27]. Based on the results shown in Fig. 6, we determined the optimum deposition conditions (deposition time=24 h, particle concentration=7.5×10^8 particles mL^{-1}), in which AgNP@SiO$_2$ particles (surface coverage=$11 \pm 1\%$) were well distributed on the membrane surface without forming large aggregate clusters. The particle surface coverage of 11% corresponds to the total weight of SiO$_2$ per unit membrane area of 6.435 µg cm^{-2} (see the Supporting information S5). The following characterization of membrane properties, performance and antibacterial activity was performed with the membrane prepared with the optimized deposition conditions.

The water contact angle of the pristine TFC, TFC-SH and TFC-AgNP@SiO$_2$ membranes are presented in Fig. 7. The pristine TFC membrane showed a contact angle of $68 \pm 3°$, which is within the range of values reported in the literature [19]. The water contact angle was not significantly altered after the cysteamine treatment. The TFC-AgNP@SiO$_2$ membrane had a lower water contact angle ($54 \pm 4°$) than that of the pristine TFC, which is consistent with the previous studies showing that the incorporation of AgNPs on the membrane surface reduced the water contact angle [19,20]. Improved hydrophilicity of the TFC-AgNP@SiO$_2$ membrane (decreased water contact angle) is expected to be beneficial for both minimizing the loss of water flux upon particle
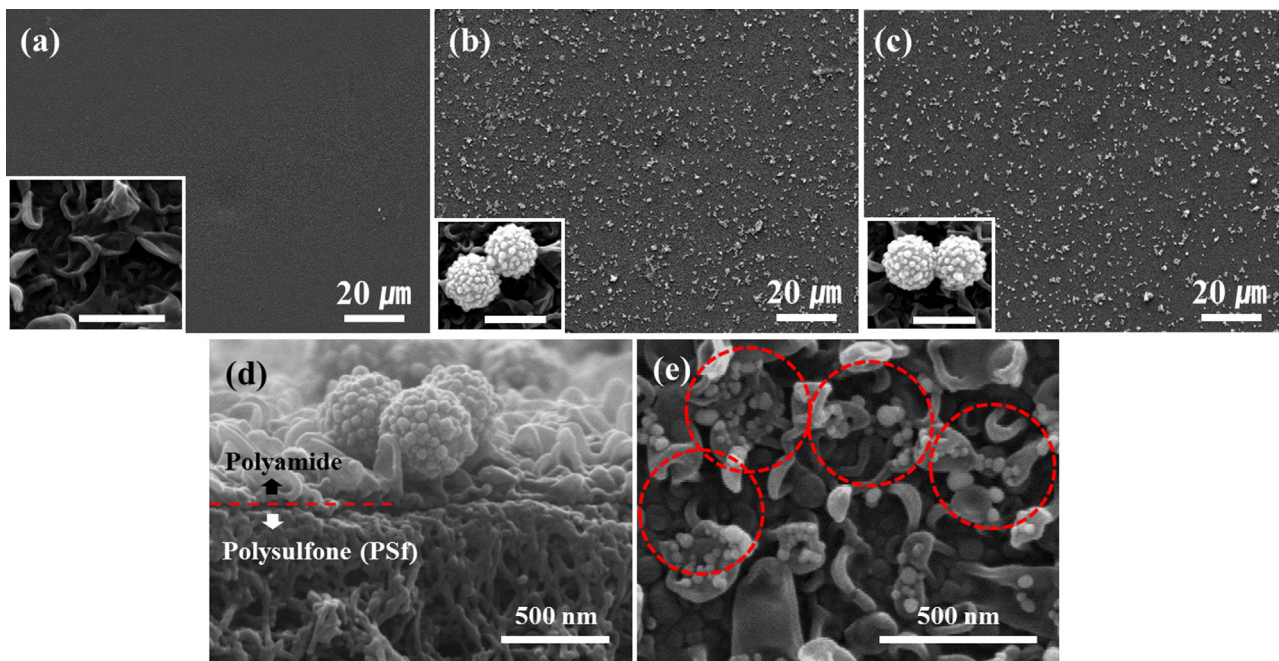
Fig. 5. SEM images of (a) the pristine TFC surface, (b) TFC-AgNP@SiO$_2$ surface, (c) TFC-AgNP@SiO$_2$ surface (after performance test), (d) TFC-AgNP@SiO$_2$ cross-section and (e) TFC-AgNP@SiO$_2$ surface (after sonication). The TFC-AgNP@SiO$_2$ was prepared with the particle concentration of 7.5×10^8 particles mL^{-1} and 24 h deposition time. Scale bars in inset images denote 500 nm.

deposition and alleviating biofouling by reducing bacterial adhesion on the membrane surface [38,39].

3.3. Membrane performance

The water flux and NaCl rejection of the pristine TFC, TFC-SH and TFC-AgNP@SiO$_2$ membranes are shown in Fig. 8. Both water flux and NaCl rejection remain essentially unchanged by the sequential surface modifications, cysteamine functionalization and AgNP@SiO$_2$ immobilization, within the errors arising from sample preparation and measurement. As a result, the TFC-AgNP@SiO$_2$ membrane exhibited NaCl rejection of $98.8 \pm 0.2\%$ along with water flux of 29 ± 2 L m^{-2} h^{-1}, comparable to those of the pristine TFC ($99.0 \pm 0.1\%$, 30 ± 2 L m^{-2} h^{-1}). Yin et al. reported a significant decline in NaCl rejection after cysteamine treatment performed in an ethanol medium, which is likely associated with the partial destruction of the PA network by ethanol [20]. The unchanged NaCl rejection after membrane modifications in this
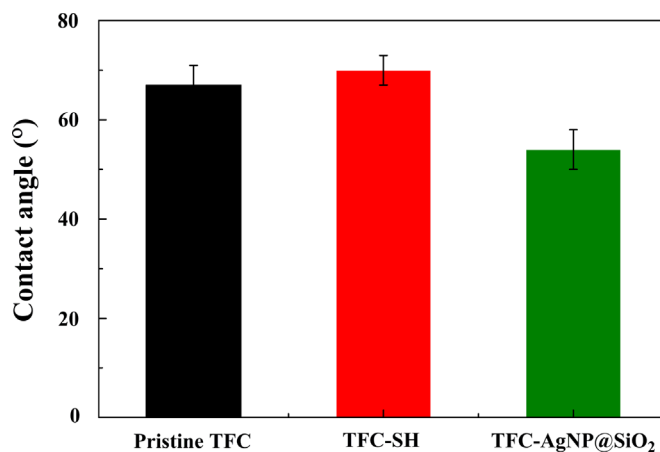
Fig. 7. Water contact angle of the pristine TFC, TFC-SH and TFC-AgNP@SiO$_2$ membranes.
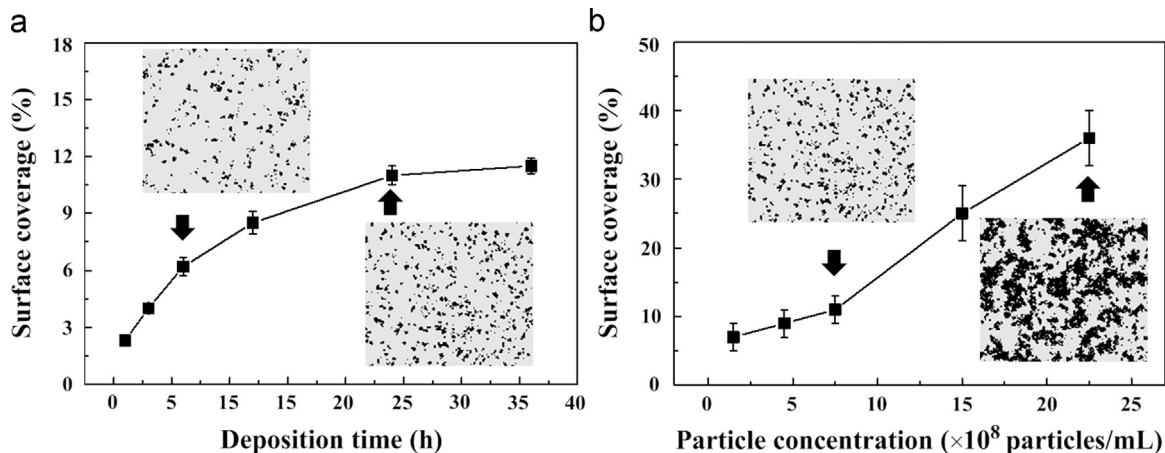
Fig. 6. The surface coverage of the TFC-AgNP@SiO$_2$ membrane by AgNP@SiO$_2$ particles as a function of (a) particle deposition time (at the fixed AgNP@SiO$_2$ concentration=7.5×10^8 particles mL^{-1}) and (b) particle concentrations (at the fixed deposition time=24 h).
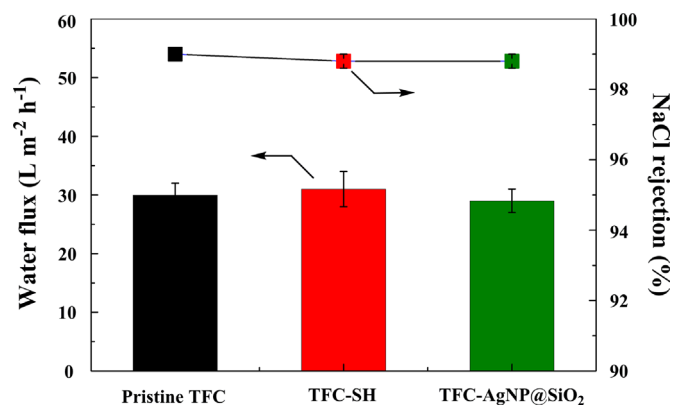
Fig. 8. Water flux and NaCl rejection of the pristine TFC, TFC-SH and TFC-AgNP@SiO$_2$ membranes.

study is ascribed mainly to the use of the aqueous media for cysteamine functionalization, which prevents PA damage due to the much lower swelling power of water for PA compared to ethanol [40]. Negligible loss of water flux even after AgNP@SiO$_2$ immobilization can be explained by the good distribution and low surface coverage (11 ± 1%) of the particles. This morphology can provide little resistance to water passage across the membrane, unlike other AgNP-immobilized membranes that suffer from greatly increased hydraulic resistance upon AgNP deposition [18,22]. Furthermore, the improved wettability (reduced water contact angle) by AgNP@SiO$_2$ immobilization could possibly compromise the increase in transport resistance. The negligible impact of AgNP@SiO$_2$ immobilization on the membrane performance demonstrates the merit of our approach to functionalize NPs on the membrane surface.

3.4. Membrane antibacterial property

Antibacterial properties of the fabricated membranes were evaluated *via* the viable cell attachment experiment for three types of model bacteria, *E. coli*, *P. aeruginosa* and *S. aureus*. Fig. 9 shows the number of live bacteria attached on the pristine TFC, TFC-SH and TFC-AgNP@SiO$_2$ membranes. The results showed that the TFC-SH has some antibacterial property by reducing the number of viable *E. coli*, *P. aeruginosa* and *S. aureus* cells by

17.3 ± 1.5, 13.3 ± 0.7 and 45.9 ± 0.4%, respectively, after 2 h contact. It has recently been reported that sulfur and sulfur-containing compounds show a potential as antimicrobial agents [41]. When bacteria adhere to the sulfur-containing compounds, they lose their morphological integrity with a decrement in the growth rate, which finally leads to bacterial death [41]. Hence, the observed antibacterial properties of the TFC-SH are likely to be imparted by the presence of the antimicrobial sulfur on its surface. On the other hand, the TFC-AgNP@SiO$_2$ membrane exhibited a significant reduction in the number of live bacteria by 92.7 ± 1.8, 99.5 ± 0.3 and 73.3 ± 5.5% for *E. coli*, *P. aeruginosa* and *S. aureus*, respectively, compared to the pristine TFC, demonstrating its strong antibacterial properties against both gram-negative (*E. coli* and *P. aeruginosa*) and gram-positive bacteria (*S. aureus*).

The strong antibacterial effect on the modified membrane surface was further confirmed by the fluorescence microscopy image of the membranes incubated in bacteria solutions as shown in Fig. 10. The fluorescence microscopy images revealed that the adhesion and biofilm growth of all the bacteria were restricted for the TFC-AgNP@SiO$_2$ membrane compared to the pristine membrane. In addition, the TFC-AgNP@SiO$_2$ membrane clearly exhibited the strong ability of killing bacteria as manifested in the higher portion of dead cell (red color) on its surface. Qualitatively, the antibacterial effect of the TFC-AgNP@SiO$_2$ was the highest for *P. aeruginosa* and the lowest for *S. aureus*, which is in good agreement with the quantitative results as described in Fig. 9.

The membrane antibacterial effect in the bacteria solution was also assessed by counting the number of colony of the supernatant bacteria solution after removing the membranes as shown in Fig. 11. The colony formation was remarkably suppressed and only a few colonies were observed for the TFC-AgNP@SiO$_2$, indicating its strong antibacterial effect. The bacterial viability was calculated using the culture plate images to quantify the antibacterial effect as shown in Fig. 12. The bacterial viability of the TFC-AgNP@SiO$_2$ membrane was estimated to be 7.9%, 0.3% and 19.1% for *E. coli*, *P. aeruginosa* and *S. aureus*, respectively. This tendency of the bacterial viability in the solution depending on the bacteria type is qualitatively similar to that of the antibacterial activity on the membrane surface as shown in Fig. 9.

Although the antibacterial mechanism of AgNPs has not yet been completely elucidated, commonly accepted mechanisms include (1) cell membrane damage by direct contact of AgNPs, followed by disturbance of the permeability and respiration,
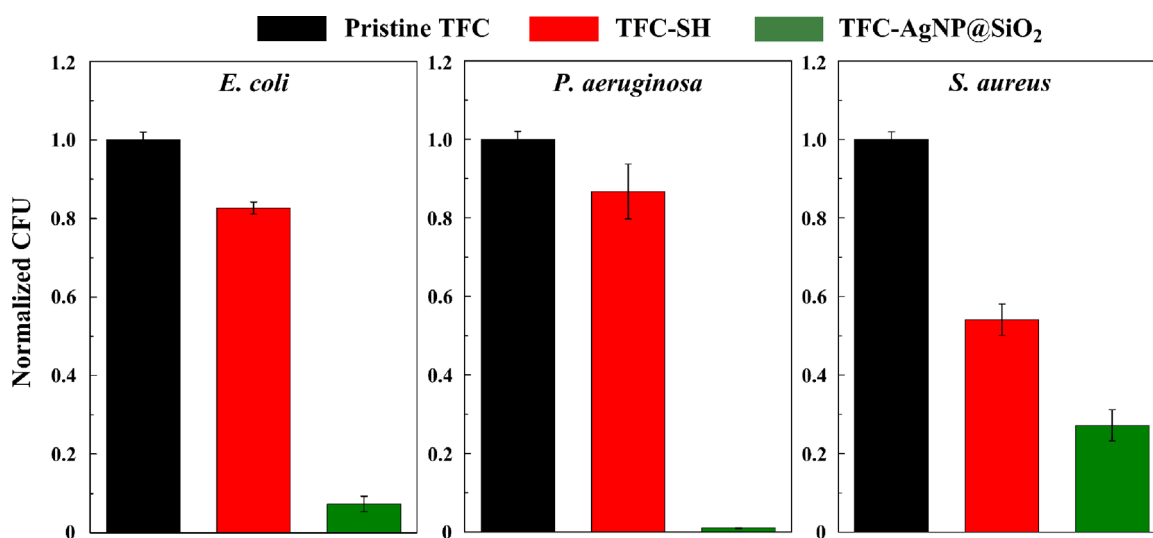
Fig. 9. The normalized number of live bacteria attached on the pristine TFC (black), TFC-SH (red) and TFC-AgNP@SiO$_2$ (green) membranes for gram-negative (*E. coli* and *P. aeruginosa*) and gram-positive (*S. aureus*) bacteria. The values were normalized by the number of live bacteria attached on the pristine TFC. (For interpretation of the references to color in this figure legend, the reader is referred to the web version of this article.)
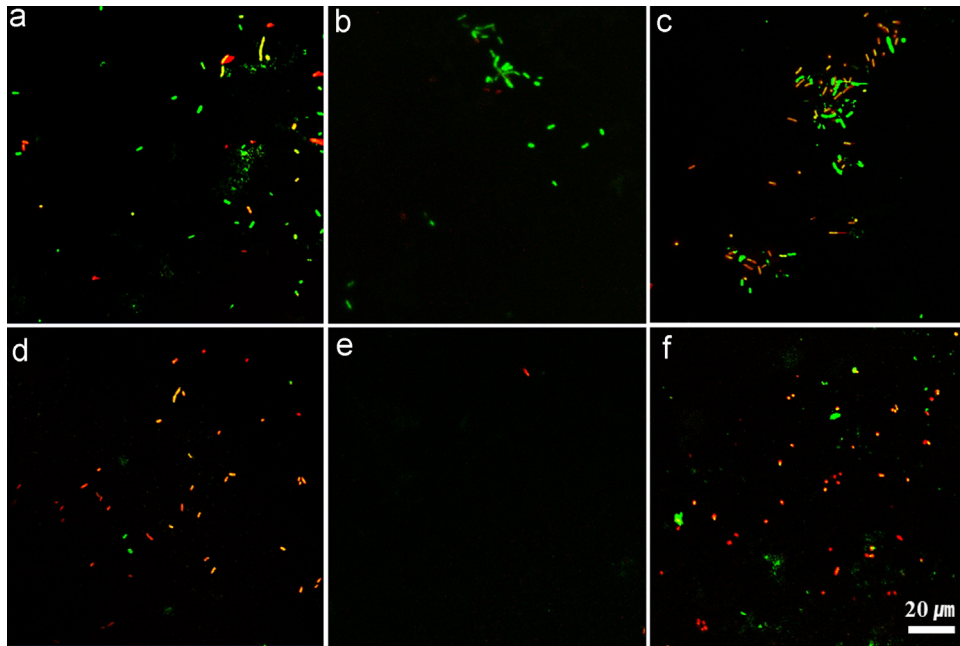
Fig. 10. Fluorescence microscopy images of (a and d) *E. coli*, (b and e) *P. aeruginosa* and (c and f) *S. aureus* on the (a–c) pristine TFC and (d–f) TFC-AgNP@SiO₂ membranes. Live cells are stained green, while dead ones are stained red. (For interpretation of the references to color in this figure legend, the reader is referred to the web version of this article.)

(2) generation of reactive oxygen species by AgNPs and free Ag^+ ions and (3) disruption of adenosine triphosphate (ATP) production and DNA replication by penetration of released Ag^+ ions [5,42]. The strong antibacterial activity of the TFC-AgNP@SiO₂ even with a relatively low particle coverage of ~11%, is attributed to the good and effective distribution of the SiO₂ particles densely-
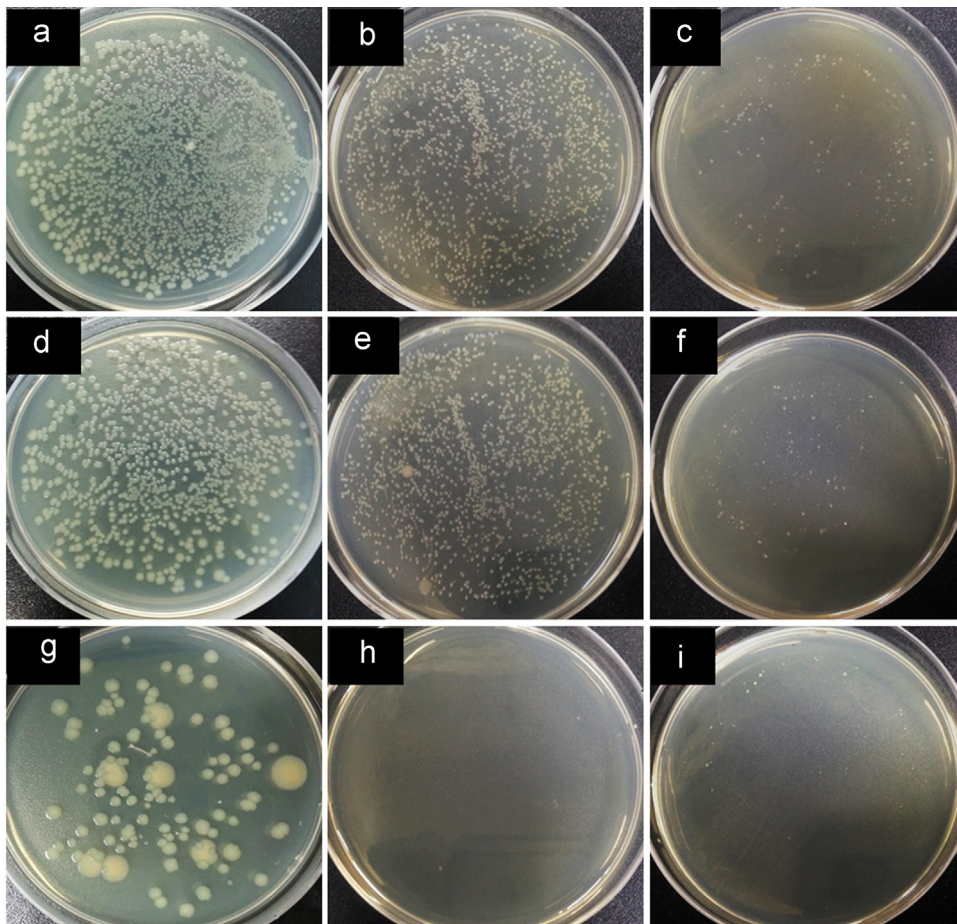
Fig. 11. Photographs of the bacterial culture plates of (a, d, g) *E. coli*, (b, e, h) *P. aeruginosa* and (c, f, i) *S. aureus* for the (a–c) control, (d–f) pristine TFC membranes and (g–i) TFC-AgNP@SiO₂ membranes. Control denotes the blank bacteria culture without being contacted with membranes.
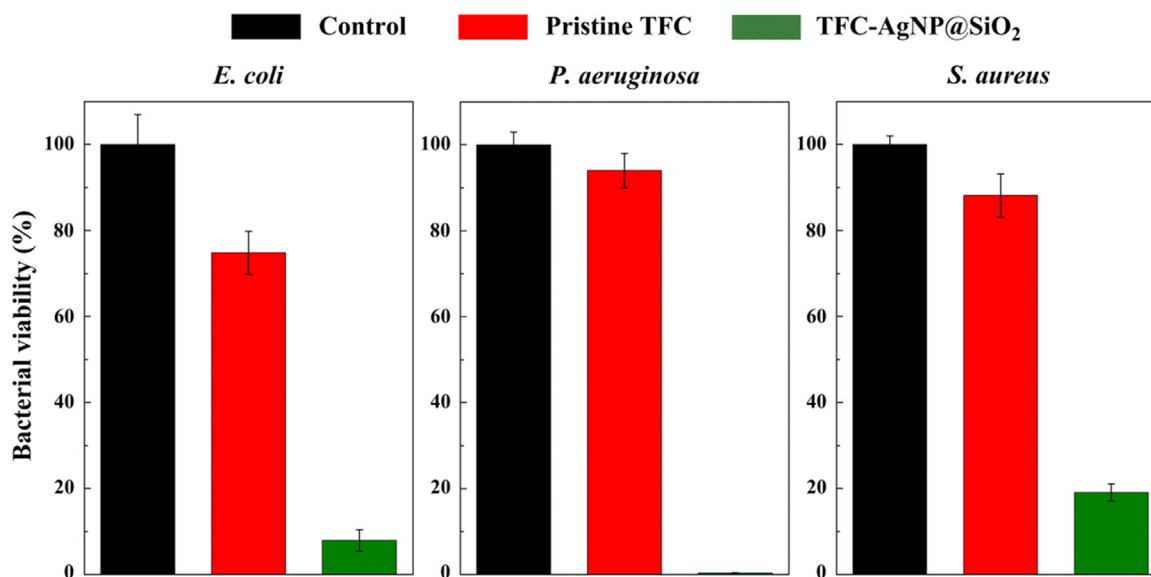
Fig. 12. Bacterial viability of the control (black), pristine TFC membrane (red) and TFC-AgNP@SiO$_2$ membrane (green) against *E. coli*, *P. aeruginosa* and *S. aureus*. Control denotes the blank bacteria culture without being contacted with membranes. (For interpretation of the references to color in this figure legend, the reader is referred to the web version of this article.)

packed with biocidal AgNPs, which can enlarge the contact of AgNPs with bacteria and allow the effective elution of Ag$^+$ ions. In addition, the enhanced hydrophilicity of the TFC-Ag@SiO$_2$ membrane could further contribute to the antibacterial performance by reducing bacterial adhesion on the membrane surface. It is interesting to note that the TFC-AgNP@SiO$_2$ membrane showed stronger antibacterial activity for gram-negative bacteria than for gram-positive bacteria. This can be explained by the difference in the cell wall constituents of gram-negative versus gram-positive bacteria with respect to the biocidal effect of AgNPs. The cell wall of gram-positive bacteria is primarily comprised of a thick peptidoglycan layer ($\sim$30 nm) covered with appendages, while gram-negative bacteria have cells consisting of a thinner peptidoglycan layer ($-$10 nm) [43]. Hence, AgNPs and Ag$^+$ ions are presumed to more readily impair and penetrate a thinner peptidoglycan layer, respectively, leading to more destruction of transport and respiratory proteins and disruption of DNA replication. Consequently, a more pronounced antibacterial effect is present for the gram-negative bacteria [16].

3.5. Releasing behavior of Ag$^+$ ions

The long-lasting antibacterial effect is preferred for practical membrane applications, and the releasing dynamics of Ag$^+$ ions from the Ag-incorporated membrane is directly related to the duration of the antibacterial activity. Hence, we evaluated the release rate of Ag$^+$ ions from the TFC-AgNP@SiO$_2$ membrane following the protocol reported previously [20]. Fig. 13 shows the release rate of Ag$^+$ ions and the weight percentage of the Ag remaining on the TFC-AgNP@SiO$_2$ membrane. A relatively large amount of Ag$^+$ ions (0.018 μg cm^{-2}) was released out during the first day, which corresponds to a weight loss of $\sim$11.6% based on the total amount of Ag loaded on the membrane (0.155 μg cm^{-2}). After the first day, the release rate of Ag$^+$ ions rapidly decreased to reach a steady state value of $\sim$0.0011 μg cm^{-2} day^{-1}, corresponding to a weight loss of $\sim$0.7% per day. The high initial release rate of Ag$^+$ ions, followed by its rapid reduction is consistent with the observations reported by other researchers [20,44]. Such a low steady release rate would be linked to the strong bonds between the AgNPs and SiO$_2$ particles and between the AgNP@SiO$_2$ particles and the membrane surface, along with the low particle
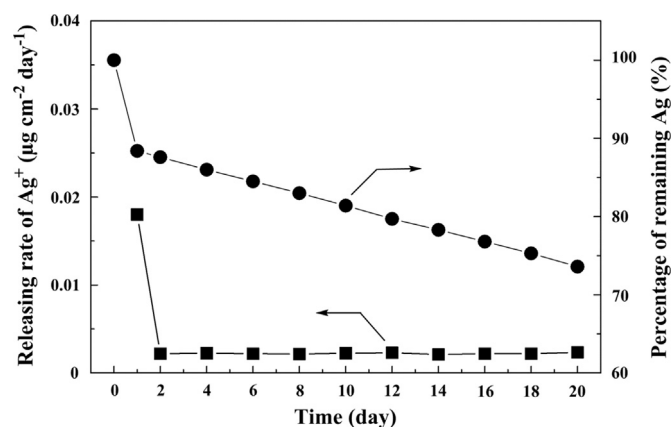
Fig. 13. Releasing rate of Ag$^+$ ions from the TFC-AgNP@SiO$_2$ membrane and the weight percentage of Ag remaining on the membrane.

loading. The weight loss of Ag after 20 days was estimated to be $\sim$26.4%. When we consider the steady release rate of Ag$^+$ ions, the antibacterial activity of the membrane is expected to last more than 140 days. The duration of the antibacterial effect for 140 days may be insufficient to prolong the membrane lifetime significantly. Work is currently underway to control the release rate of Ag$^+$ ions by modifying the surface of AgNP@SiO$_2$ particles, which enables the antibacterial effect to last longer than 1 year. It should be important to note that any trace of Ag$^+$ ions were not detected (below 0.1 ppb, the detection limit of ICP-MS) for the releasing test in 3.0 wt% NaCl solution simulating seawater for 20 days. The remarkable suppression in the release rate of Ag$^+$ ions is attributed to the possible formation of AgCl passivation layer on the AgNP surface in the presence of NaCl [45]. This result infers that the antibacterial activity of AgNPs would last longer than 140 days expected based on the releasing experiment in pure water, although their antibacterial strength is expected to be diminished. Throughout the releasing experiment, silica was not detected in the solution, further confirming the excellent stability of silica particle.

It is also interesting to note that the total Ag amount of our AgNP@SiO$_2$-immobilized membrane (0.155 μg cm^{-2}) is 100 times lower than that of the AgNP-immobilized membrane (15.5 μ

g cm^{-2}) reported by others [20]. Again, the excellent antibacterial activity of our TFC-AgNP@SiO$_2$ membrane with a relatively low Ag content suggests that AgNPs are effectively immobilized on the membrane in a manner that minimizes the use of Ag for long-lasting control of biofouling.

4. Conclusions

We strongly and effectively immobilized AgNP@SiO$_2$ particles on PA TFC RO membranes by forming multiple Ag − S chemical bonds between the particles and the membrane surface, thereby ensuring excellent stability of the immobilized particles (AgNPs and AgNP@SiO$_2$). The AgNP@SiO$_2$-immobilized membrane showed strong, wide-spectrum and long-lasting antibacterial activity without deteriorating the membrane performance (water flux and salt rejection). This key merit of our strategy is attributed to the good distribution of relatively large SiO$_2$ particles densely-packed with AgNPs along with the use of mild immobilization protocol. This result demonstrates that our proposed strategy to immobilize NPs could be an effective pathway in imparting various functionalities including antifouling and antibacterial properties to the membranes.

Acknowledgements

Appendix A. Supplementary material

Supplementary data associated with this article can be found in the online version at http://dx.doi.org/10.1016/j.memsci.2015.09.060.

References

[1] K.P. Lee, T.C. Arnot, D. Mattia, A review of reverse osmosis membrane materials for desalination: development to date and future potential, J. Membr. Sci. 370 (2011) 1–22.
[2] I.J. Roh, A.R. Greenberg, V.P. Khare, Synthesis and characterization of interfacially polymerized polyamide thin films, Desalination 191 (2006) 279–290.
[3] O. Akin, F. Temelli, Probing the hydrophobicity of commercial reverse osmosis membranes produced by interfacial polymerization using contact angle, XPS, FTIR, FE-SEM and AFM, Desalination 278 (2011) 387–396.
[4] R. Bernstein, S. Belfer, V. Freger, Bacterial attachment to RO membranes surface-modified by concentration-polarization-enhanced graft polymerization, Environ. Sci. Technol. 45 (2011) 5973–5980.
[5] A. Matin, Z. Khan, S.M.J. Zaidi, M.C. Boyce, Biofouling in reverse osmosis membranes for seawater desalination: phenomena and prevention, Desalination 281 (2011) 1–16.
[6] S.Y. Lee, H.J. Kim, R. Patel, S.J. Im, J.H. Kim, B.R. Min, Silver nanoparticles immobilized on thin film composite polyamide membrane: characterization, nanofiltration, antifouling properties, Polym. Adv. Technol. 18 (2007) 562–568.
[7] M. Elimelech, W.A. Phillip, The future of seawater desalination: energy, technology, and the environment, Science 333 (2011) 712–717.
[8] J. Wu, C. Yu, Q. Li, Regenerable antimicrobial activity in polyamide thin film nanocomposite membranes, J. Membr. Sci. 476 (2015) 119–127.
[9] Q. Li, S. Mahendra, D.Y. Lyon, L. Brunet, M.V. Liga, D. Li, P.J.J. Alvarez, Antimicrobial nanomaterials for water disinfection and microbial control: potential applications and implications, Water Res. 42 (2008) 4591–4602.
[10] M. Zhang, K. Zhang, B.D. Gusseme, W. Verstraete, R. Field, The antibacterial

[11] and anti-biofouling performance of biogenic silver nanoparticles by lactobacillus fermentum, Biofouling 30 (2014) 347–357.
[11] F. Diagne, R. Malaisamy, V. Boddie, R.D. Holbrook, B. Eribo, K.L. Jones, Polyelectrolyte and silver nanoparticle modification of microfiltration membranes to mitigate organic and bacterial fouling, Environ. Sci. Technol. 46 (2012) 4025–4033.
[12] M. Ben-Sasson, K.R. Zodrow, Q. Genggeng, Y. Kang, E.P. Giannelis, M. Elimelech, Surface functionalization of thin-film composite membranes with copper nanoparticles for antimicrobial surface properties, Environ. Sci. Technol. 48 (2014) 384–393.
[13] S. Leong, A. Razmjou, K. Wang, K. Hapgood, X. Zhang, H. Wang, TiO$_2$ based photocatalytic membranes: a review, J. Membr. Sci. 472 (2014) 167–184.
[14] Q. Li, S.-L. Chen, W.-C. Jiang, Durability of nano ZnO antibacterial cotton fabric to sweat, J. Appl. Polym. Sci. 103 (2007) 412–416.
[15] F. Perreault, M.E. Tousley, M. Elimelech, Thin-film composite polyamide membranes functionalized with biocidal graphene oxide nanosheets, Environ. Sci. Technol. 1 (2014) 71–76.
[16] M. Rai, A. Yadav, A. Gade, Silver nanoparticles as a new generation of antimicrobials, Biotechnol. Adv. 27 (2009) 76–83.
[17] A. Mollahosseini, A. Rahimpour, A new concept in polymeric thin-film composite nanofiltration membranes with antibacterial properties, Biofouling 29 (2013) 537–548.
[18] M.S. Rahaman, H. Therien-Aubin, M. Ben-Sasson, C.K. Ober, M. Nielsen, M. Elimelech, Control of biofouling on reverse osmosis polyamide membranes modified with biocidal nanoparticles and antifouling polymer brushes, J. Mater. Chem. B 2 (2014) 1724–1732.
[19] S. Zhang, G. Qiu, Y.P. Ting, T.S. Chung, Silver-PEGylated dendrimer nanocomposite coating for anti-fouling thin film composite membranes for water treatment, Colloids Surf. A 436 (2013) 207–214.
[20] J. Yin, Y. Yang, Z. Hu, B. Deng, Attachment of silver nanoparticles (AgNPs) onto thin-film composite (TFC) membranes through covalent bonding to reduce membrane biofouling, J. Membr. Sci. 441 (2013) 73–82.
[21] E.P. Chan, W.D. Mulhearn, Y.-R. Huang, J.-H. Lee, D. Lee, C.M. Stafford, Tailoring the permselectivity of water desalination membranes via nanoparticle assembly, Langmuir 30 (2014) 611–616.
[22] M. Ben-Sasson, X. Lu, E. Bar-Zeev, K.R. Zodrow, S. Nejati, G. Qi, E.P. Giannelis, M. Elimelech, In situ formation of silver nanoparticles on thin-film composite reverse osmosis membranes for biofouling mitigation, Water Res. 62 (2014) 260–270.
[23] Y.-S. Ko, Y.H. Joe, M. Seo, K. Lim, J. Hwang, K. Woo, Prompt and synergistic antibacterial activity of silver nanoparticle-decorated silica hybrid particles on air filtration, J. Mater. Chem. B 2 (2014) 6714–6722.
[24] H. Nakatsuji, J.-I. Morita, T. Misaki, Y. Tanabe, Water solvent method for esterification and amide formation between acid chlorides and alcohols promoted by combined catalytic amines: synergy between N-Methylimidazole and N,N,N′,N′-tetramethyethylenediamine (TMEDA), Adv. Synth. Catal. 348 (2006) 2057–2062.
[25] E. Faure, C. Falentin-Daudre, T.S. Lanero, C. Vreuls, G. Zocchi, C. Van De Weerdt, J. Martial, C. Jerome, A.S. Duwez, C. Detrembleur, Functional nanogels as platforms for imparting antibacterial, antibiofilm, and antiadhesion activities to stainless steel, Adv. Funct. Mater. 22 (2012) 5271–5282.
[26] B.P. Tripathi, N.C. Dubey, S. Choudhury, F. Simon, M. Stamm, Antifouling and antibiofouling pH responsive block copolymer based membranes by selective surface modification, J. Mater. Chem. B 1 (2013) 3397–3409.
[27] A.M. El Badawy, T.P. Luxton, R.G. Silva, K.G. Scheckel, M.T. Suidan, T. M. Tolaymat, Impact of environmental conditions (pH, ionic strength, and electrolyte type) on the surface charge and aggregation of silver nanoparticles suspensions, Environ. Sci. Technol. 44 (2010) 1260–1266.
[28] R. Heffernan, A.J.C. Semiao, P. Desmond, H. Cao, A. Safari, O. Habimana, E. Casey, Disinfection of a polyamide nanofiltration membrane using ethanol, J. Membr. Sci. 448 (2013) 170–179.
[29] S.L. Miller, G. Schlesinger, Prebiotic syntheses of vitamin coenzymes: I. Cysteamine and 2-mercaptoethanesulfonic acid (Coenzyme M), J. Mol. Evol. 36 (1993) 302–307.
[30] M. Wirde, U. Gelius, Self-assembled monolayers of cystamine and cysteamine on gold studied by XPS and voltammetry, Langmuir 15 (1999) 6370–6378.
[31] G. Kang, H. Yu, Z. Liu, Y. Cao, Surface modification of a commercial thin film composite polyamide reverse osmosis membrane by carbodiimide-induced grafting with poly(ethylene glycol) derivatives, Desalination 275 (2011) 252–259.
[32] V.T. Do, C.Y. Tang, M. Reinhard, J.O. Leckie, Degradation of polyamide nanofiltration and reverse osmosis membranes by hypochlorite, Environ. Sci. Technol. 46 (2012) 852–859.
[33] K. Boussu, J.D. Baerdemaeker, C. Dauwe, M. Weber, K.G. Lynn, D. Depla, S. Aldea, I.F.J. Vankelecom, C. Vandecasteele, B.V. Bruggen, Physico-chemical characterization of nanofiltration membranes, ChemPhysChem 8 (2008) 370–379.
[34] H.H. Park, S. Park, G. Ko, K. Woo, Magnetic hybrid colloids decorated with Ag nanoparticles bite away bacteria and chemisorb viruses, J. Mater. Chem. B 1 (2013) 2701–2709.
[35] S.Y. Park, J.W. Chung, Y.K. Chae, S.-Y. Kwak, Amphiphilic thiol functional linker mediated sustainable antibiofouling ultrafiltration nanocomposite comprising a silver nanoparticles and poly(vinylidene fluoride) membrane, ACS Appl. Mater. Interfaces 5 (2013) 10705–10714.
[36] B.J.R. Thio, J.-H. Lee, J.C. Meredith, Characterization of ragweed pollen adhesion to polyamides and polystyrene using atomic force microscopy, Environ.

Sci. Technol. 4433 (2009) 4308–4313.

[37] J. Liu, D.A. Sonshine, S. Shevani, R.H. Hurt, Controlled release of biologically active silver from nanosilver surfaces, ACS Nano 4 (2010) 6903–6913.

[38] J. Nikkola, X. Liu, Y. Li, M. Raulio, H.-L. Alakomi, J. Wei, C.Y. Tang, Surface modification of thin film composite RO membrane for enhanced anti-bio-fouling performance, J. Membr. Sci. 444 (2013) 192–200.

[39] I. Sawada, R. Fachrul, T. Ito, Y. Ohmukai, T. Maruyama, H. Matsuyama, Development of a hydrophilic polymer membrane containing silver nanoparticles with both organic antifouling and antibacterial properties, J. Membr. Sci. 387 – 388 (2012) 1–6.

[40] J.S. Louie, I. Pinnau, M. Reinhard, Effects of surface coating process conditions on the water permeation and salt rejection properties of composite polyamide reverse osmosis membranes, J. Membr. Sci. 367 (2011) 249–255.

[41] S. Thakur, S. Barua, N. Karak, Self-healable castor oil based tough smart hyperbranched polyurethane nanocomposite with antimicrobial attributes, RSC Adv. 5 (2015) 2167–2176.

[42] C. Marambio-Jones, E.M.V. Hoek, A review of the antibacterial effects of silver nanomaterials and potential implications for human health and the environment, J. Nanopart. Res. 12 (2010) 1531–1551.

[43] O. Habimana, A.J.C. Semiao, E. Casey, The role of cell-surface interactions in bacterial initial adhesion and consequent biofilm formation on nanofiltration/reverse osmosis membranes, J. Membr. Sci. 454 (2014) 82–96.

[44] X. Cao, M. Tang, F. Liu, Y. Nie, C. Zhao, Immobilization of silver nanoparticles onto sulfonated polyethersulfone membranes as antibacterial materials, Colloids Surf. B 81 (2010) 555–562.

[45] K. Loza, J. Diendorf, C. Sengstock, L. Ruiz-Gonzalez, J.M. Gonzalez-Calbet, M. Vallet-Regi, M. Koller, M. Epple, The dissolution and biological effects of silver nanoparticles in biological media, J. Mater. Chem. B 2 (2014) 1634–1643.